Applied Composite Materials (2021) 28:1291–1313
https://doi.org/10.1007/s10443-021-09914-x

Experimental Study on the Seismic Performance of Columns Reinforced by the CFRP Bar and Sheet

Jun Zhao[1] · Wenbo Ren[1] · Xiaohui Ruan[2] · Xinglong Gong[3] · Chenzhe Si[2]

Received: 19 November 2020 / Accepted: 17 May 2021 / Published online: 29 May 2021

Abstract
To analyze the influence of CFRP (Carbon Fiber Reinforced Polymer) reinforcement ratio and CFRP sheet on the self-centering performances of concrete circular columns, five concrete circular columns were tested under the low-cyclic reversed load in this work. The five concrete circular columns included 1 RC (Reinforced Concrete) column, 2 CFRP bars reinforced concrete circular columns and 2 CFRP bars reinforced concrete circular columns with CFRP sheet strengthening partially. The hysteretic curves, skeleton curves, stiffness degradation, strength degradation, residual deformations, energy dissipation and ductility of the five circular columns were obtained and analyzed to verify the improvement of the seismic performances of the specimens reinforced with CFRP bars and CFRP sheets. At the same time, the reference opinions for practical applications of CFRP bars and CFRP sheets in structures can be provided. The test results showed that the bearing capacity and deformation capacities of the concrete circular columns reinforced with CFRP bars were 25.5% and 25% higher than that of the RC column, respectively. The deformation capacities, energy consumption capacities and deformation recovery capacities of CFRP bars reinforced concrete circular columns with CFRP sheet strengthening partially were 21.5%, 40% and 78.5% higher than that of the RC column, respectively.

Keywords CFRP bars · CFRP sheets · Concrete column · Self-centering · Seismic performance

1 Introduction

Building structures designed by current standards might be severely damaged after the earthquake, which could cause huge economic losses and arduous post-disaster reconstruction projects. Therefore, the serviceability of building structures after the

✉ Xiaohui Ruan
rxiaohui@zzu.edu.cn

[1] School of Civil Engineering, Zhengzhou University, Zhengzhou 450001, Henan, P.R. China

[2] School of Mechanics and Safety Engineering, Zhengzhou University, Zhengzhou 450001, Henan, P.R. China

[3] CAS Key Laboratory of Mechanical Behavior and Design of Materials, Department of Modern Mechanics, University of Science and Technology of China, Hefei 230027, Anhui, P.R. China

earthquake was increasingly concerned [1]. In 2009, American and Japanese researchers collectively determined that future anti-seismic researches were focused on the repairability of the building structures [2]. Studies showed that the maintenance cost of the building would be much greater than the reconstruction cost of the building when the residual interstory drift was over 0.5% [3]. So, it was necessary to carry out the researches on how to reduce the residual interstory drift of the buildings after the earthquake.

Deformation would occur in the structures under earthquake and could be eliminated by reinforcement with prestressing or special tendon. This kind of structure was called the self-centering structure. Currently, self-centering structural systems had been applied in practical engineering projects [4–6]. Priestley and MacRae [7] carried out the test about the seismic performance of the post-tensioned prestressed rocking beam-column joint and the test results showed that the seismic performances of the well-designed beam-column joint specimens were better. Ricles et al. [8] conducted research on self-resetting steel frame structures and the post-tensioned prestressed tendons had been used to provide restoring forces for the specimens. The results indicated that the self-resetting structures could effectively reduce the residual deformation of specimens. Researches about the seismic performance of unbonded prestressed concrete self-centering shear walls had been carried out by Kurama et al. [9, 10]. The results showed that the shear walls had a good self-centering capacity and almost had no damage even when the lateral deformation of the shear wall was large. Sun and Funato [11] tested 6 ultra-high-strength steel bars reinforced concrete columns under high axial load and low-cyclic reversed load. The results showed that the residual deformations of the specimens were inconspicuous. Gu et al. [12] assembled various types of energy dissipation dampers into self-centering reinforced concrete shear walls to remedy the shortcomings of low energy dissipation in self-centering structural systems [13, 14]. The test results indicated that the deformation and self-centering capacities of the new type of self-centering hybrid shear walls were better. Lee and Billington [15] evaluated the seismic performance of the self-centering concrete bridge system and found out that the residual deformation of the self-centering concrete bridge system was small and the mechanical behavior of the self-centering concrete bridge system was well after the earthquake.

Carbon Fiber Reinforced Polymer was frequently applied in concrete structures by processing into bars and sheets because of its high tensile strength and good corrosion resistance [16–19]. CFRP bars were made of heating multiple strand carbon fiber bundles which were saturated and covered high-performance resin-based materials. CFRP bars had high tensile strength and good corrosion resistance and could be used as reinforcing steel bars to improve the mechanical behavior of the reinforced concrete structures [20–22]. Zhang et al. [23] performed low-cyclic reversed load tests on three CFRP and steel bars hybrid reinforced concrete beams. The test results showed that the ductility performances of the hybrid reinforced beams were better. Sharbatdar [24] carried out the tests of 10 CFRP reinforced concrete columns under low-cyclic reversed load. The test results indicated that the carrying and deformation capacity of the CFRP reinforced concrete columns were good. Zhong et al. [25] performed an experimental study on the seismic performance of six CFRP reinforced concrete columns. The research results showed that the recovery capabilities of the column specimens were better than that of the conventional reinforced concrete columns and the residual deformations of column specimens reduced significantly. Zhao et al. [26] directed the experimental study on the seismic performance of CFRP reinforced concrete shear walls. The test results showed that CFRP bars could effectively improve the lateral carrying capacity of the concrete shear wall and the residual deformations of the specimens reduced simultaneously.

The CFRP sheets were usually used to improve the carrying and deformation capacity of the reinforced concrete structures because of the high strength and elasticity modulus [27–29]. In the 1990s, CFRP sheets were widely used for experimental study on the seismic strengthening of structures in the United States. The seismic performances of CFRP reinforced concrete bridge columns were researched by Hamid [30]. The results indicated that the carrying capacity of bridge columns had been greatly improved by reinforced with CFRP bars; the lateral carrying and deformation capacity of bridge columns were effectively enhanced by CFRP bars. The research results of Zhong et al. [25] and Saqan et al. [31] showed that externally wrapped CFRP sheets could not only effectively reduce the residual deformations of the specimens but also effectively increase the energy dissipation. Wang et al. [32, 33] completed low-cyclic reversed load and simulated seismic load tests on concrete column specimens wrapped with CFRP sheets to confirm the effect of CFRP sheets on seismic behavior. The column specimens revealed satisfactory ductility and load capacity. Wang et al. [34] carried out the study of 11 concrete columns reinforced with CFRP sheets and found that the number of layers of externally wrapped CFRP sheets had little effect on the stiffness of the concrete columns. Ye et al. [35] summarized the results of 8 CFRP sheets reinforced concrete columns under low-cyclic reversed load. The strong constraint effect of CFRP sheets had been confirmed. It was worth mentioning that CFRP sheets also had the restorative function on the damaged reinforced concrete structure. Saljoughian and Mostofinejad [36] jointly studied the grooving method of CFRP reinforcement to prevent CFRP strips prematurely off the concrete substrate and the grooving method considerably enhanced the carrying capacities of specimens compared with the conventional externally bonded reinforcement technique. Afterward, Saljoughian and Mostofinejad [37] have finished the research of seismic strengthening of square reinforced concrete columns; the results show that specimens with the grooving method of CFRP reinforcement have greater carrying capacity ductility and energy dissipation capacity. The destructive columns reinforced with CFRP sheets still had good energy dissipation capacity in Zhang's tests [38].

In this paper, five concrete circular columns reinforced with CFRP bars and CFRP sheets were tested under the low-cyclic reversed load to research the improvement of CFRP bars and CFRP sheets on the self-centering of specimens. The phenomena and crack development of the columns were recorded and researched to verify the inhibition of CFRP bars and CFRP sheets on the crack development of specimens. The hysteresis curves, skeleton curves, stiffness degradation, strength degradation, residual deformation, and energy consumption capabilities of the specimens were systematically analyzed to research the seismic performance of the concrete circular columns reinforced with CFRP bars and CFRP sheets.

2 Experimental Program

2.1 Specimens Design

The material properties of the steel bars, concrete, CFRP bars, and CFRP sheets that were used in the tests were shown in Tables 1, 2 and 3. The comparison of CFRP bars and sheets was shown in Fig. 1 and the stress-strain curves of the HRB400 steel bars and CFRP were shown in Fig. 2.

The concrete compressive strength in 28th day as shown in Table 1 was determined by the actual measured value: the test includes 12 concrete cubes with a side length of 150

Fig. 1 The CFRP bar and CFRP sheet for testing

mm and the reference standard was the Chinese Standard "Standard for evaluation of concrete compressive strength GB50107-2010" [39]. The standard deviation of the concrete compressive strength was 2.094 which was calculated according to the Chinese Standard. Part of the mechanical properties of CFRP bars and CFRP sheets were provided by the manufacturer and the actual tensile strength was measured due to the importance of design parameters as shown in Table 2. 6 samples for each different kind of reinforcement as shown in Table 3 and the results were meet the specification [40].

The tests were divided into two groups to research the effect of different CFRP bars substitution rates and wrapped CFRP sheets on the seismic performance of specimens. Totally, five columns with the same geometric dimensions were prepared. The concrete column was constituted by the bottom beam (1250 mm × 450 mm × 500 mm), the circular column (Φ350 mm × 1120 mm) and the head beam (500 mm × 450 mm × 400 mm). The specific dimensions of specimens were shown in Fig. 3 [40].

HRB400 steel bars (12 mm-diameter) and CFRP bars were used as the longitudinal bars and uniformly distributed at the circular section. Longitudinal bars of the bottom beam and the head beam were 16 mm-diameter HRB400 steel bars. The stirrups were 12 mm-diameter HRB400 steel bars. The stirrup spacings of the foundation beam and the head beam were 120

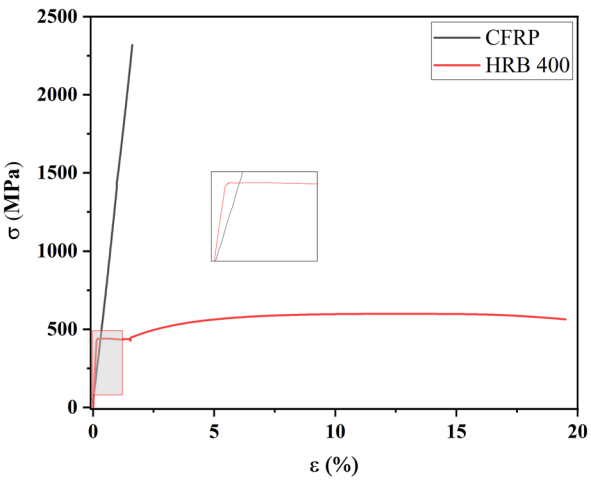

Fig. 2 The stress-strain curves of the HRB400 steel bars and CFRP

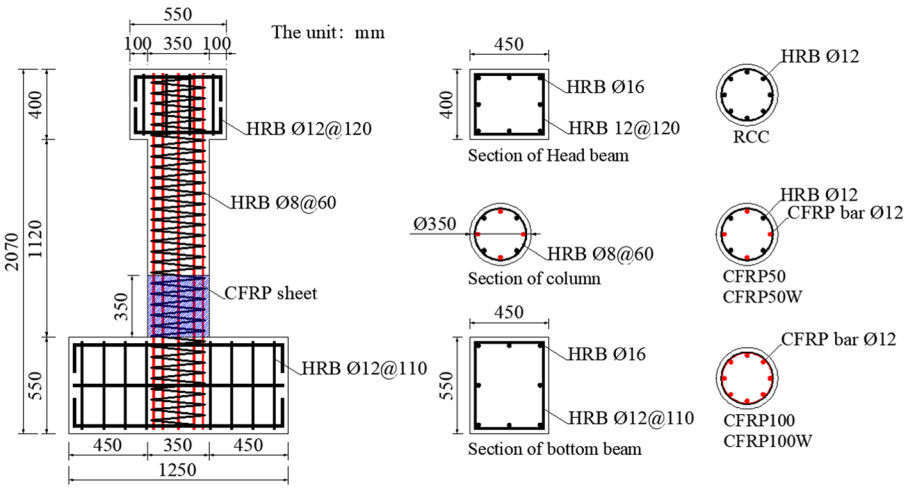

Fig. 3 The size and reinforcement layout of the specimen (unit: mm)

mm and 110 mm, respectively. The height of the circular column was 1120 mm and the diameter was 350 mm. The type of stirrup of the column was spiral stirrup which was made of 8 mm-diameter HRB400 steel bars with a stirrup spacing of 60 mm. The thickness of the concrete cover was 25 mm. The parameters of the specimens were shown in Fig. 3 and Table 4.

The specimen named RCC meant conventional reinforced concrete column, CFRP50 meant CFRP bars substitution rate was 50%, CFRP100 meant CFRP bars substitution rate was 100%, CFRP50W meant CFRP bars substitution rate was 50% and wrapped with CFRP sheets, CFRP100W meant CFRP bars substitution rate was 100% and wrapped with CFRP sheets.

2.2 Specimens Preparation

The production process of the specimen was mainly divided into the following steps: cutting CFRP bars and steel bars according to the reinforcement design, anchoring CFRP bars, finishing reinforcement cages, pasting strain gauges of reinforcing bars, pouring and curing concrete.

CFRP bars were high-strength reinforced bars, so the anchors were very important in order to give full play to its high tensile capacity in the specimens. Bond-type anchors were adopted in this paper and the main components of the anchors were steel sleeve pipes, high-strength adhesion agents and steel plates. High-strength Q345 steel was used for manufacturing materials of steel sleeve pipes and steel plates, the inner diameter of the pipe

Table 1 The composition and strength of concrete

Water-cement ratio	Cement grade	Cement (kg)	Water (kg)	Fine aggregate (kg)	Coarse aggregate (kg)	Compressive strength (MPa)
0.47	42.5	394 (16.4%)	185 (7.7%)	571 (23.8%)	1250 (52.1%)	34.9

Table 2 The mechanical properties of CFRP sheets

Tensile strength (GPa)	Tensile elastic modulus (GPa)	Bending strength (MPa)	Shear strength (MPa)	Surface density (g/m^2)	Thickness (mm)	Elongation (%)
3.6	233	736	46	292	0.167	1.62

was 28 mm and the pipe wall thickness was 3 mm. High-strength grouting concrete with a great performance of rapid moisture-releasility and self-compactness was used as high-strength adhesion agents. The specific anchoring method was shown in Fig. 4.

The anchorage length of CFRP bar was 330 mm and the ultimate tensile strength of CFRP bar was about 2300 MPa. The anchoring method can effectively prevent CFRP bars withdraw from the anchor: the failure mode of all testing CFRP bar samples was CFRP fracture instead of anchors failure. The details were shown in Fig. 5.

CFRP50W and CFRP100W specimens were wrapped with CFRP sheets and the reinforcement height was 350 mm. The total length of CFRP sheet was 1300 mm including the perimeter of the circular column was 1100 mm and the splicing length of CFRP sheets was 200 mm [41]. The reinforcement method of the specimen was single-layer CFRP sheets. Specimen surface was polished and kept dry and flat to ensure the reinforcement direction was the same as the stickup direction. Epoxy resin flooring primer was applied to the surface of specimens and assembly glue painted on the reinforcement area.

2.3 Loading Protocols and Testing Content

The testing apparatuses were constituted by a horizontal loading actuator, a vertical loading hoisting jack, a reaction frame, two jacks, four ground anchors and two steel beams. To ensure the vertical loading hoisting jack gliding smoothly during the test, the connection system which made up of the slideways and the sliding blocks was used between the vertical loading hoisting jack and the reaction frame. A special custom-made connection device was used as the connection between the specimens and the horizontal loading actuator. The connection device could meet the requirement of connection strength and guarantee the ball joint twisting freely. The jacks could limit the horizontal swipe of specimens and the ground anchors-steel beams system could limit the vertical swipe of specimens. The testing apparatuses were shown in Fig. 6.

After specimens were installed, the location of the vertical loading hoisting jack was adjusted to ensure the vertical axial force which was 382.8 kN could be steadily imposed

Table 3 The mechanical properties of CFRP bars and steel reinforcement

Type	Diameter (mm)	Yield strength (MPa)	Yield strain ($\mu\varepsilon$)	Ultimate strength (MPa)	Elasticity modulus (MPa)
HRB400	8	531	2636	644	2.01×10^5
HRB400	12	426	2147	575	1.98×10^5
HRB400	16	445	2187	603	2.03×10^5
CFRP	12	\	\	2310.2	1.43×10^5

on specimens until the end of the experiment. The vertical axial force was calculated from the 0.15 axial compression ratio and the calculation formula (1) as followed:

$$N = 0.76 \times \mu \times a \times f_c \tag{1}$$

Where 0.76 was the conversion factor of cubic compressive strength and prism compressive strength; μ was the axial compression ratio; a was the cross-sectional area of the column; f_c was the compressive strength of concrete [40].

Low-cyclic lateral loading was applied on the specimens through the horizontal loading actuator based on the designed experimental loading process. The interstory drift 0.25% corresponds to 3.3 mm, 0.5% corresponds to 6.6 mm, and so on. The loading process was shown in Fig. 7.

During the tests, two cycles were applied at each drift level with increments of 0.25% up to 2.5%. In subsequent loading, one cycle was applied at the drift levels of 3.0% to 7.0%, respectively. The loading rate was 0.33 mm/s and the loading rate of loading and unloading were equal [42]. Until the lateral carrying capacity of the test specimen dropped to 85% of the maximum carrying capacity or the specimen was destroyed, the tests were completed. The load and displacement of horizontally loading actuators were collected by a static acquisition instrument, the horizontal and vertical displacements corresponding to different heights of concrete columns were collected by a YHD-type displacement meter, the strain of longitudinal bars and stirrups were collected by strain gauges, the concrete strain and the crack width were also recorded. The arrangement of displacement measuring points was shown in Fig. 8.

The uppermost displacement meter was located at the middle of the head beam used to measure the horizontal displacement of the loading actuator. The displacement meters of columns were divided into eight groups and each group contained a vertical displacement meter and a horizontal displacement meter. The displacement meters respectively were located at 50 mm, 350 mm, 650 mm and 950 mm from the bottom of the column, as shown in Fig. 8.

3 Experimental Results and Discussion

The seismic performances of CFRP bars reinforced concrete circular columns with CFRP strengthening partially were systematically studied by analyzing the failure mode, hysteresis curves, skeleton curves, stiffness degradation, strength degradation, residual deformation, and energy dissipation capacity of the columns.

3.1 Failure Mode

The development of cracks and the failure form was carefully recorded during the tests. The overall test process was roughly summarized into three stages. Firstly, the horizontal cracks appeared and developed with the increase of interstory drift. Secondly, vertical cracks appeared and residual deformation increased. Finally, the lateral carrying capacities of the specimens were reduced and the concrete at the root of the column was spalled. In order to compare the effect of different CFRP bars substitution rate and CFRP sheets on the seismic performance of concrete circular columns clearly, test results were divided into two parts: the columns with different CFRP bars substitution rate and the columns reinforced with and without CFRP sheets. The failure modes of 5 specimens were shown in Fig. 9.

Table 4 The parameters of the specimens

Name	RCC	CFRP50	CFRP100	CFRP50W	CFRP100W
CFRP bars substitution rate	0%	50%	100%	50%	100%
longitudinal bars	8 HRB400 bars	4 CFRP bars and 4 HRB400 bars	8 CFRP bars	4 CFRP bars and 4 HRB400 bars	8 CFRP bars
axial compression ratio	0.15	0.15	0.15	0.15	0.15
CFRP sheets strengthening	no	no	no	yes	yes

From the test results, it could be seen that the development of the cracks for RCC, CFRP50 and CFRP100 specimens were similar. The failure types of the three specimens were bending failures under the horizontal loads and vertical loads. The failure interstory drifts for the three specimens were 4%, 5%, and 5%, respectively. The test results indicated that the failure interstory drifts for the three specimens were greater than the elastic-plastic interstory drift angle limitation of frame construction (2%) which was stipulated in the "Technical Specification for Concrete Structure of Tall Building" (JGJ3-2010, Chinese Standard) [43]. For the three different specimens, the first horizontal crack with a width of 0.02 mm appeared when the interstory drifts were 0.25% and located at 160 mm, 272 mm, and 256 mm from the bottom of the columns, respectively. The cracks were closed during the unloading phase of the tests because the columns were in the elastic stage at this time.

The horizontal cracks gradually developed with the increase of interstory drift. The crack distribution area of RCC specimen was 750 mm and that of CFRP100 specimen was 885 mm from the column bottom. The first residual cracks of RCC specimen, CFRP50 specimen and CFRP100 specimen appeared when the interstory drifts were 0.5%, 0.75% and 1%, respectively. The first vertical crack of RCC specimen appeared when the interstory drift was 2.0% and the first vertical cracks of CFRP50 specimen and CFRP100 specimen appeared when the interstory drift was 2.5%. It indicated that the recovery capabilities of the specimen increased when it was reinforced by CFRP bars. So, CFRP bars could effectively prevent premature cracking damage of concrete. The peak load of the

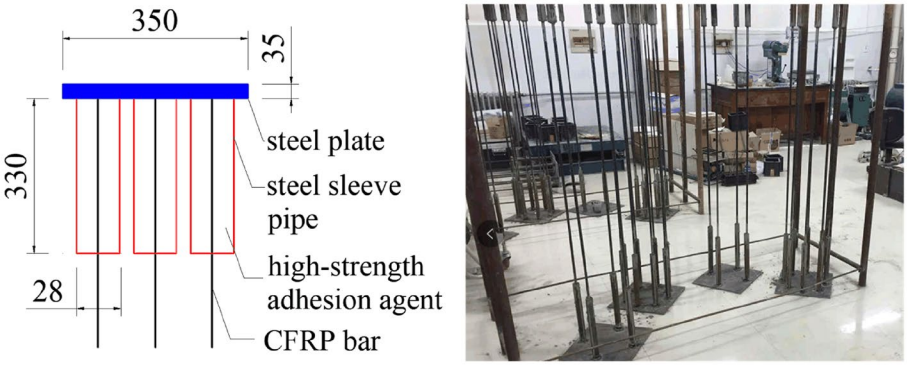

Fig. 4 The anchoring method of CFRP bars (unit: mm)

Fig. 5 The failure mode of CFRP bars

RCC specimen was 87.2 kN at the interstory drift of 2%. The peak loads of CFRP50 and CFRP100 specimens appeared when the interstory drifts were 4%, and the peak loads were 95.7 kN and 109.4 kN, respectively.

Vertical cracks continued developing in the late test and concrete in the lower part began to damage at the same time. The bottom concrete of RCC specimen was extensive damage when the interstory drift was 3.0% and those of the CFRP50 and CFRP100 specimens were 4.0%. The test was considered to be stopped when the horizontal load declined to 85% of the peak load. The failure loads of the three specimens were 71.8 kN, 59.7 kN and 87.5 kN, respectively. At this time, the maximum crack width of the RCC specimen was 2.52 mm and the residual crack width was 1.41 mm, the maximum crack width of the CFRP50 specimen was 2.57 mm and the residual crack width was 0.96 mm, the maximum crack width of the CFRP100 specimen was 2.31 mm and the residual crack width was 0.72 mm. At failure, RCC specimen had relatively obvious residual cracks and residual deformations compared with CFRP50 specimen and CFRP100 specimen. Compared with RCC, the residual deformation of CFRP100 specimen was decreased by 48.9%. The height of the concrete crushing zone of the RCC specimen was 190 mm which was obviously smaller than 250 mm of CFRP50 specimen and 260 mm of CFRP100 specimen.

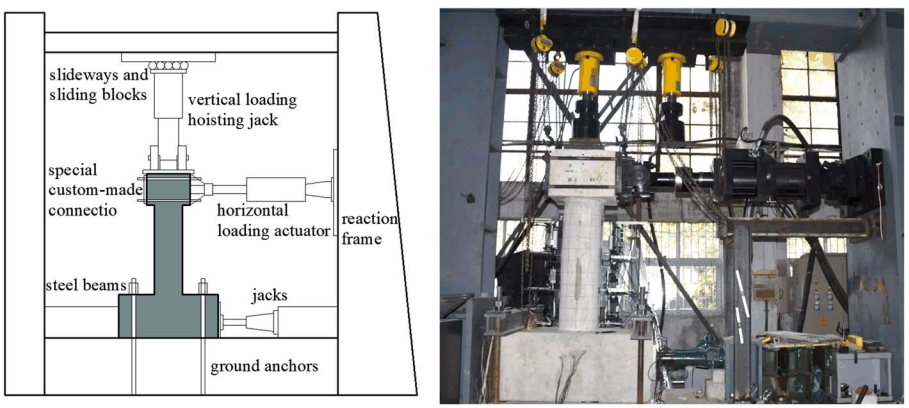

Fig. 6 The testing apparatus

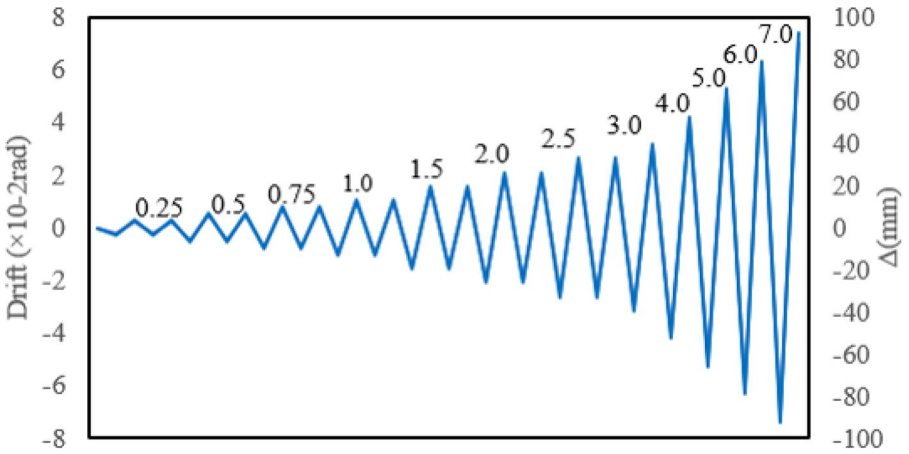

Fig. 7 The loading processes

CFRP50W specimen and CFRP100W specimen had stronger constraining forces of plastic hinge due to reinforcement of CFRP sheets. This reinforcement method could upgrade the ultimate interstory drift to 7%. The crack could only be measured within the unwrapped area because of the envelope of CFRP sheets. The first cracks appeared when

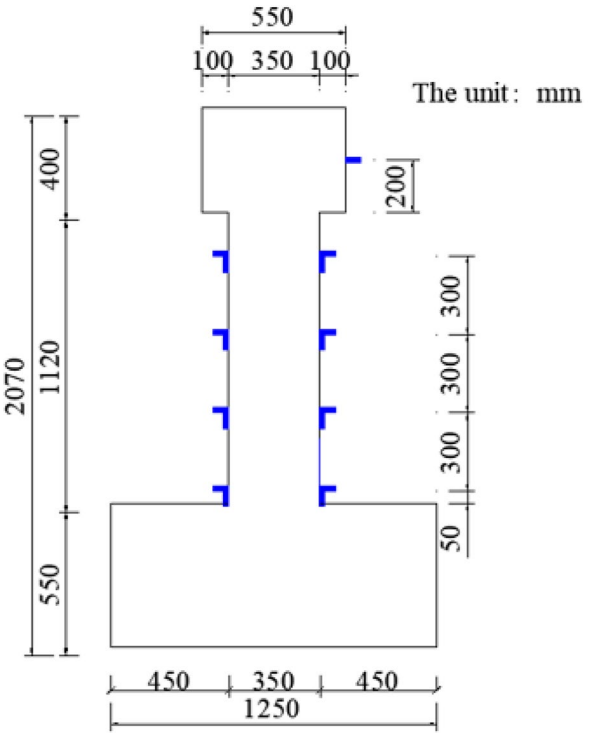

Fig. 8 The arrangement of displacement measuring points (unit: mm)

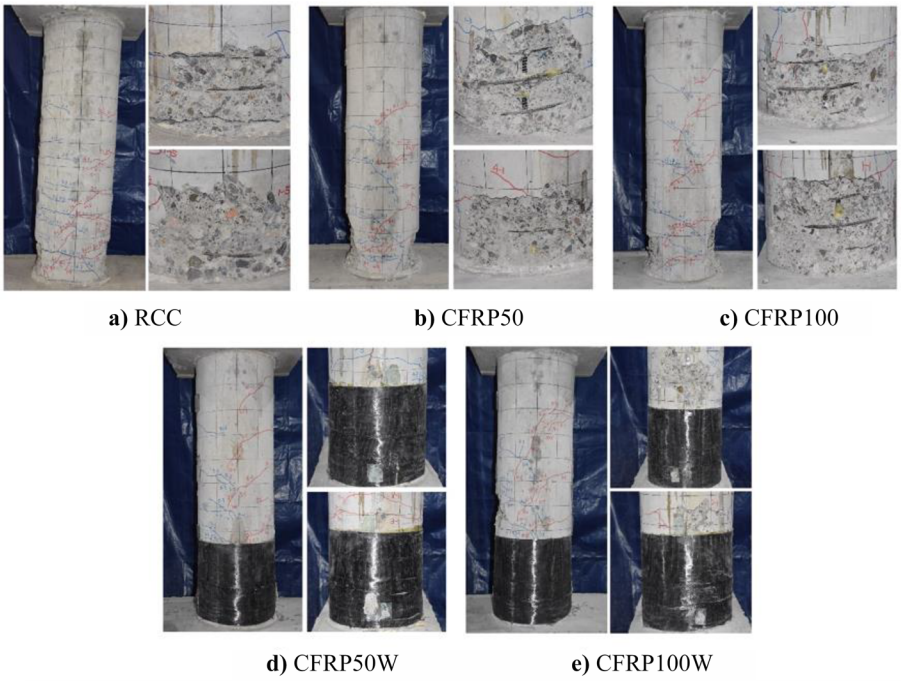

Fig. 9 The failure mode of 5 concrete circular columns

the interstory drifts were 0.5% for both CFRP50W and CFRP100W. The height of the crack was 400 mm and the width was 0.02 mm.

The horizontal cracks developed rapidly in the middle of the test and the distribution area of horizontal cracks of CFRP sheets reinforced specimen was 900 mm. The first residual cracks of CFRP50W specimen and CFRP100W specimen were observed at the interstory drift of 1%. The sound of CFRP sheets tearing can be heard and inconspicuous damage can be observed in the late test stage. Horizontal cracks continue to develop. However, there was no obvious spalling of concrete because the reinforced with CFRP sheets. The peak load of CFRP50W specimen was 106.1 kN at the interstory drift of 6%, and the peak load of CFRP100W specimen was 132.9 kN at the interstory drift of 7%.

The failure loads for CFRP50W and CFRP100W specimens were 90.8 kN and 90.2 kN, respectively. The maximum crack width of CFRP50W specimen was 2.41 mm and the residual crack width was 0.68 mm. The maximum crack width of CFRP100W specimen was 2.42 mm and the residual crack width was 0.65 mm. At the end of the test, CFRP sheets were cracked and the residual deformations of both specimens were small. It could be proved that the CFRP sheets had strong constraints on the plastic hinge. CFRP sheets reinforcement could effectively improve the recovery capabilities of the specimens and significantly increase the carrying capacity of the specimens. Compared with CFRP50 and CFRP100 specimens, CFRP50W and CFRP100W specimens had significantly improved deformation capacities of the columns. Details of cracks development of each specimen were described in Table 5.

Table 5 The crack development and carrying capacity of each specimen

Name	RCC	CFRP50	CFRP100	CFRP50W	CFRP100W
Interstory drift of the first crack (mm)	0.25	0.25	0.25	0.25	0.5
Interstory drift of the first vertical crack (mm)	0.5	0.75	1	\	\
Ultimate interstory drift (%)	4	5	5	7	7
Maximum crack width (mm)	2.52	2.57	2.31	2.41	2.42
Residual crack width (mm)	1.41	0.96	0.72	0.68	0.65
Carrying capacity (kN)	87.2	95.7	109.4	106.1	132.9

3.2 Hysteresis Curves

The hysteresis curves of five specimens were shown in Fig. 10. The hysteretic curve of the RCC specimen was plumper which meant that more seismic energy could be dissipated during the earthquake. The hysteresis curve of CFRP50 specimen was a little pinching and that for CFRP100W was more obvious compared with RCC specimen. The linear elasticity of CFRP bars resulted in that the curve decreased rapidly during the unloading stage. So, the residual deformations of CFRP bars reinforced concrete columns under the same loading were smaller. The peak loads of CFRP50 and CFRP100 specimens appeared comparatively late than RCC specimen. When the interlayer drift angle was 2% (Δ=26.4 mm), the load of RCC specimen increased to the peak load, then it decreased slowly. The CFRP50 and CFRP100 specimens reached peak loads when the interstory drifts were 4% (Δ=52.8 mm). The peak loads of CFRP50 and CFRP100 were 95.7 kN and 109.4 kN which were 9.7% and 25.5% larger than that of the RCC specimen, respectively. However, both CFRP50 and CFRP100 specimens showed a rapidly declining tendency of loads.

CFRP50W and CFRP100W specimens showed excellent lateral carrying capacity due to the external partially wrapped CFRP sheets reinforcement. The hysteresis curves for CFRP50W and CFRP100W specimens were plumper and the pinching phenomenon of the hysteresis curves was more mitigatory than CFRP50 and CFRP100 specimens.

In addition, the hysteresis curves of the specimens reinforced with CFRP bars did not show the ductility characteristic before failure which appeared in the hysteresis curve of the RCC specimen. This indicated that the carrying capacities of CFRP bars reinforced concrete specimens without CFRP sheets would promptly decrease after concrete spalling.

The hysteresis curves of specimens were pinched under low cycle repeated load, the pinching width ratios [47] were calculated based on experimental data. For RCC specimen, the pinching width ratio was calculated to be 0.48 when the interstory drift was 2.5%. The pinching width ratios of CFRP50, CFRP100, CFRP50W and CFRP100W respectively were 0.45, 0.5, 0.4 and 0.36. At interstory drift of 3.0%, the pinching width ratios of 5 specimens were 0.55, 0.52, 0.49, 0.42 and 0.39. The results showed that the pinching width ratios of the specimens with CFRP bars have relatively lower pinching width ratios and a more obvious pinching effect.

3.3 Skeleton Curves

The skeleton curves of the five specimens were shown in Fig. 11 which were obtained by connecting the peak points of each cycle of the hysteresis curves.

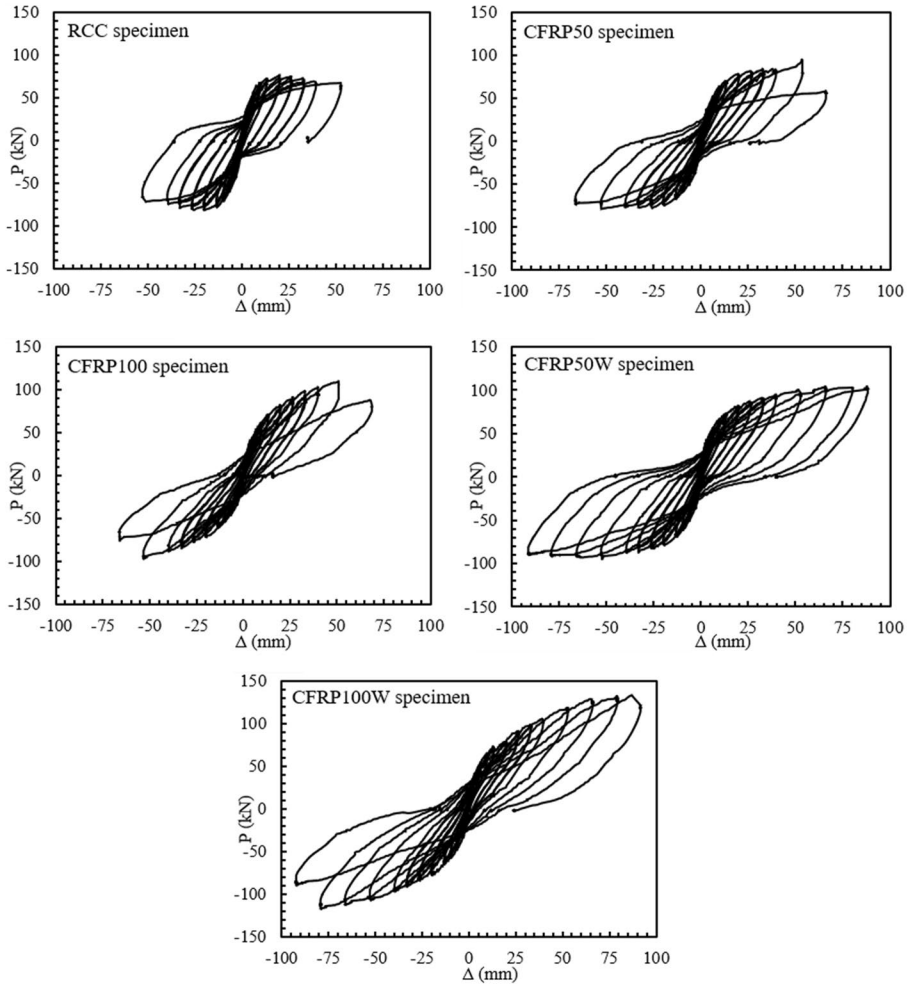

Fig. 10 The hysteresis curves of specimens

At the beginning of the test, the initial slope of all skeleton curves was large. With the increase of the load, the skeleton curve of RCC specimen showed a significant yielding state which indicated that the ductility performance of the RCC specimen was good compared with CFRP specimens. The ultimate carrying capacity and the ultimate interstory drift angle of the RCC specimen were relatively small. However, the skeleton curves of CFRP50 and CFRP100 specimens showed an escalating trend. Especially, the slope of the skeleton curve of CFRP100 specimen was large. The ultimate carrying loadings of CFRP50 and CFRP100 specimens were 95.7 kN and 109.4 kN which were 9.7% and 25.5% higher than that of the RCC specimen, respectively. After the failure of the specimens, the descending slopes of the skeleton curves of the CFRP specimens were larger than that of the RCC specimen and showed no real sign of warning before the rupture which was caused by the linear elastic property and relatively low elastic modulus of CFRP bars.

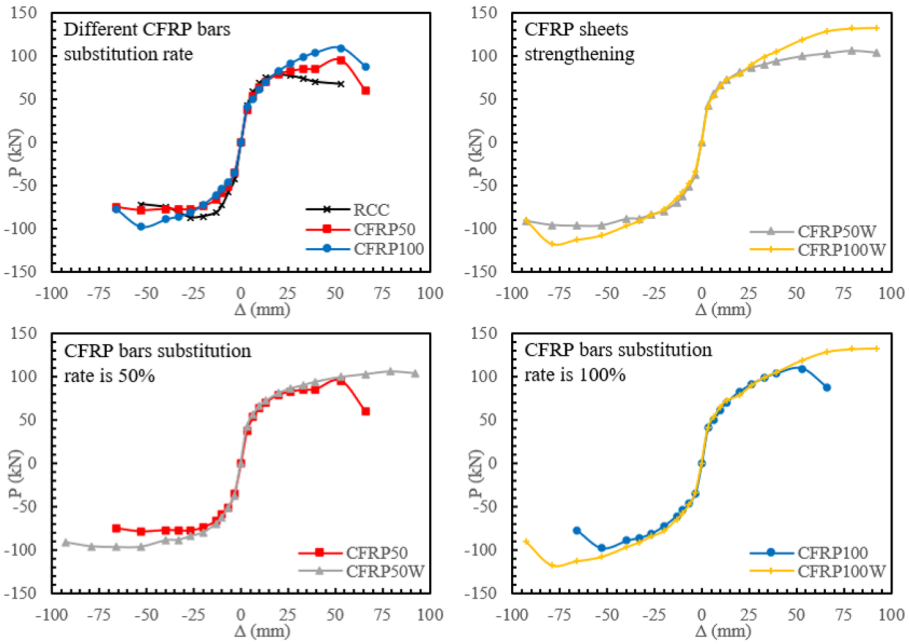

Fig. 11 The skeleton curves of specimens

The overall trends of the skeleton curves of CFRP50W and CFRP100W specimens were similar to those of CFRP50 and CFRP100 specimens. The skeleton curves of CFRP50W and CFRP100W specimens had a more obvious rising trend curve before failure when compared with the CFRP50 and CFRP100 specimens. The ultimate carrying loads of CFRP50W and CFRP100W specimens were 106.1 kN and 132.9 kN which were 10.9% and 21.5% higher than CFRP50 and CFRP100 specimen, respectively. The ultimate inter-story drifts increased to 7% (Δ=92.4 mm) which indicated that the CFRP sheets could effectively improve the carrying capacities and deformation capacities of the specimens.

3.4 The Stiffness Degradation

The slope of the hysteresis curve and the skeleton curve gradually decreased with the increase of interstory drift, which showed that the stiffness of specimens gradually degrades under low-cyclic reversed load. In this paper, secant stiffness K_i was calculated according to formula (2) specified in reference [42] and was showed in Fig. 12.

$$K_i = \frac{|+F_i| + |-F_i|}{|+X_i| + |-X_i|} \tag{2}$$

In the formula, F_i was the peak load of the i-th cycle, and X_i was the ultimate displacement of the i-th cycle, correspondingly.

From Fig. 12, it could be seen that the forms of secant stiffness degradation of all specimens were basically the same. Firstly, the secant stiffness decreased rapidly when

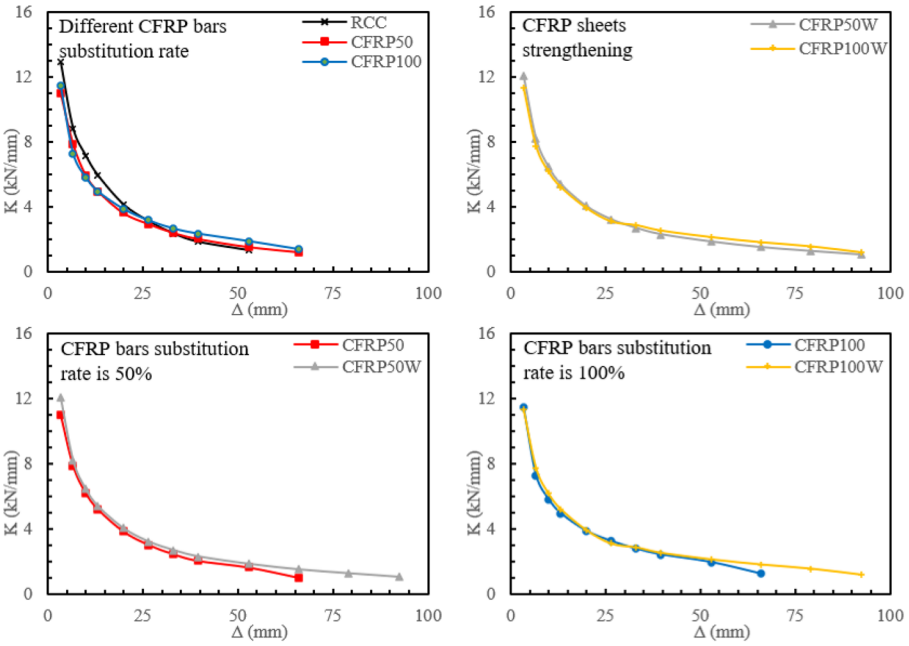

Fig. 12 The stiffness degradation of specimens

the interstory drift was less than 0.75% (Δ=9.9 mm). Then, the secant stiffness decreased slowly when the interstory drift was between 1% (Δ=13.2 mm) - 2.5% (Δ=33.0 mm). At last, the downtrend of secant stiffness tended to be stable when the interstory drift was over 2.5% (Δ=33.0 mm).

The initial stiffness of RCC specimen was 15% greater than that of the CFRP50 and CFRP100 specimens. The initial stiffness of CFRP50 and CFRP100 were almost the same. With the increase of the interstory drift, the stiffness degradation of RCC specimen deteriorated more rapidly than that of the CFRP50 and CFRP100 specimens. The stiffness degradation of CFRP100 specimen degraded slowly when the interstory drift was over 2.5% (Δ=33.0 mm). RCC specimen was damaged when the interstory drift was 4% (Δ=52.8 mm) and the residual stiffness of CFRP50 and CFRP100 specimens were 24.4% and 47.9% higher than the RCC specimen, respectively. When the interstory drift was 5% (Δ=66.0 mm), CFRP50 and CFRP100 specimens failed and the residual stiffness of CFRP100 was 22.3% higher than that of the CFRP50 specimen.

It could be found from Fig. 12 that the stiffness degradation of CFRP sheets reinforced specimens degraded more slowly than specimens without CFRP sheets specimens when the interstory drift was larger than 2.5% (Δ=33.0 mm). For example, the stiffness of the CFRP50W specimen was reduced by 44.1% compared with CFRP50 specimen was 58.6% when the interstory drift was 2.5% (Δ=33.0 mm) to 5% (Δ=66.0 mm). CFRP50 and CFRP100 specimens were broken when the interstory drifts were 5% (Δ=66.0 mm). The residual stiffnesses of CFRP50W and CFRP100W specimens were 48.3% and 47% greater than CFRP50 and CFRP100 specimen, respectively. The results showed that the CFRP sheets reinforced specimens still had stronger stiffness under large interstory drift and the CFRP sheets were proven to further improved the seismic performances of concrete columns.

3.5 The Strength Degradation

The carrying capacity of the specimen decreased with the increase of loading times when the interstory drift was the same. The degradation coefficient of carrying capacity could be represented by the ratio of the peak load at the i-th cycle to the peak load at the (i-1)-th cycle with the same interstory drift. In this paper, degradation coefficients λ_i of carrying capacity was calculated according to formula (3) which was specified in reference [42] and shown in Fig. 13.

$$\lambda_i = \frac{F_j^i}{F_j^{i-1}} \tag{3}$$

It could be seen from carrying capacity degradation coefficients curves that all specimens had great sustained loading capacity. The carrying capacity degradation coefficients of all specimens were between 0.9 and 1. The curves of strength degradation of all concrete circular columns were relatively steady and the trends of the degradation coefficient were similar.

3.6 The Residual Deformation

The residual deformation was the unrecoverable deformation of the structure after unloading and could be used to describe the self-centering capacity of the structure. The curves of residual deformations μ and interstory drifts δ were drawn according to the test results as shown in Fig. 14.

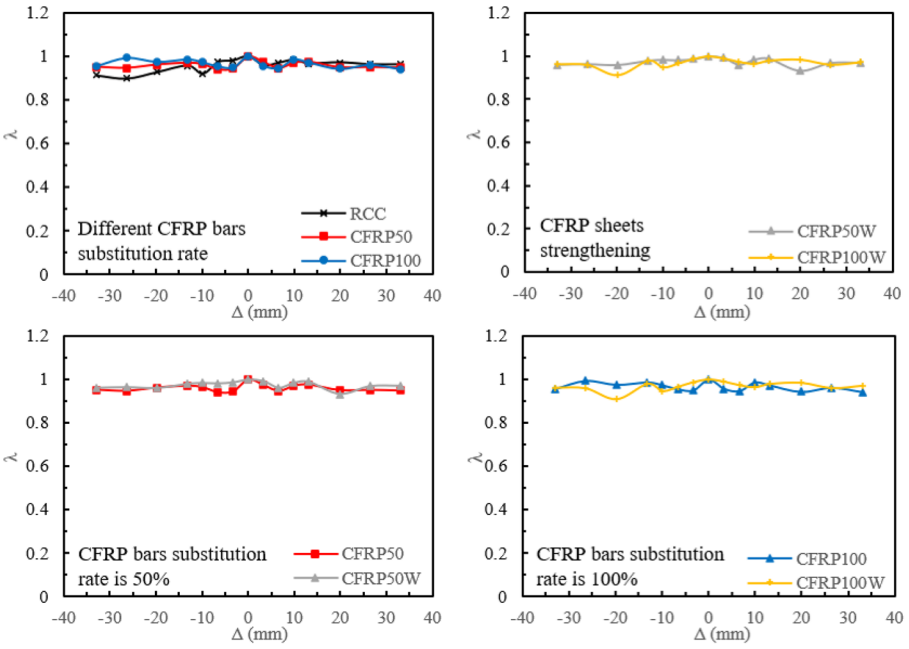

Fig. 13 The strength degradation of specimens

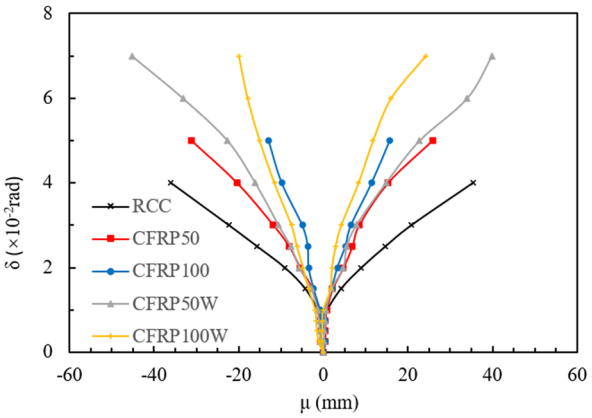

Fig. 14 The residual deformation of specimens

At the initial stage of the test, the residual deformations of specimens were relatively small and the growth rate was slow when the interstory drift was lower than 1.0% because the specimens were at the elastic stage. After that, the residual deformation of RCC specimen increased rapidly which meant the RCC specimen reached the elasto-plastic phase. By comparing the residual deformation of the specimens RCC, CFRP50 and CFRP100 under the same interstory drift, it was obviously seen that RCC specimen had the largest residual deformation, then followed by CFRP50 specimen. CFRP100 specimen had the smallest residual deformation. The residual deformations of CFRP50 and CFRP100 specimens were 13.1% and 56.3% smaller than that of the RCC specimen, respectively. The test results showed that CFRP bars could effectively control the residual deformations of the specimens and provided high self-centering capacities for the specimens.

At the same interstory drift, the residual deformation of the CFRP50W specimen was 20.5% smaller than that of the CFRP50 specimen and the residual deformation of the CFRP100W specimen was 6.3% smaller than that of the CFRP100 specimen. It was to say that the self-centering capacities of CFRP bars reinforced concrete circular columns with CFRP strengthening partially were better than other concrete circular columns. CFRP sheets could effectively control the crack development, improve the deformation capacities and increase the self-centering capacities of the specimens. The deformation recovery rates of the 5 specimens were listed in Table 6. The ratio is more representative of self-centering capacity due to the final failure deformations were different [44, 45].

Table 6 The deformation recovery rates of the 5 specimens

Specimens	RCC	CFRP50	CFRP100	CFRP50W	CFRP100W
Final failure deformation (mm)	52.8	66.0	66.0	92.4	92.4
Final residual deformation (mm)	36.0	31.3	15.7	39.9	19.9
Recovery rate (%)	31.8	52.6	76.2	56..8	78.5

Formula: $recovery\ rate = \frac{(failure\ deformation - residual\ deformation)}{failure\ deformation}$

Table 7 The calculations of energy dissipation

Specimen number	RCC	CFRP50	CFRP100	CFRP50W	CFRP100W
Cumulative energy dissipation (kN·mm)	18666.8	18896.1	16557.5	35707.3	30771.9

It could be easily seen from Table 6 that CFRP bars could provide excellent self-centering capacities for concrete circular columns and effectively control the residual deformations of the specimens, and the CFRP sheets could further increase the deformation recovery capacity of the column. In summary, CFRP bars reinforced concrete circular columns with CFRP strengthening partially could not only increase the deformation capacities but also the self-centering capacities of the columns.

3.7 The Energy Dissipation Capacity

The energy dissipation capacity was an important indicator of the seismic performance of the specimen. The intensity of energy dissipation capacity was usually measured with the size of the area enclosed by the hysteresis curves [42]. In this paper, the monocyclic area and the gross area of the hysteresis curves were calculated as shown in Table 7 and Fig. 15.

According to the analysis of Table 7, the monocyclic energy dissipation of RCC specimen was the largest. The monocyclic energy dissipation gradually decreased with the increase of CFRP bars substitution rate. The energy dissipation suddenly reduced caused by the loading process applied one cycle when the interstory drift was over 2.5%. Taking the interstory drift 3% as an example, the energy dissipation of the CFRP50 and CFRP100 specimens were 74.2% and 62.8% of RCC specimen, respectively. The results showed that the energy dissipation capacities of CFRP reinforced concrete specimens were significantly lower than that of conventional reinforced concrete specimens. The main reason for the above situation was steel bars can dissipate the seismic energy by the plastic deformation; nevertheless, CFRP bars are linear elastic materials without the yield stage. The monocyclic energy dissipation of CFRP sheets reinforced specimens were higher than

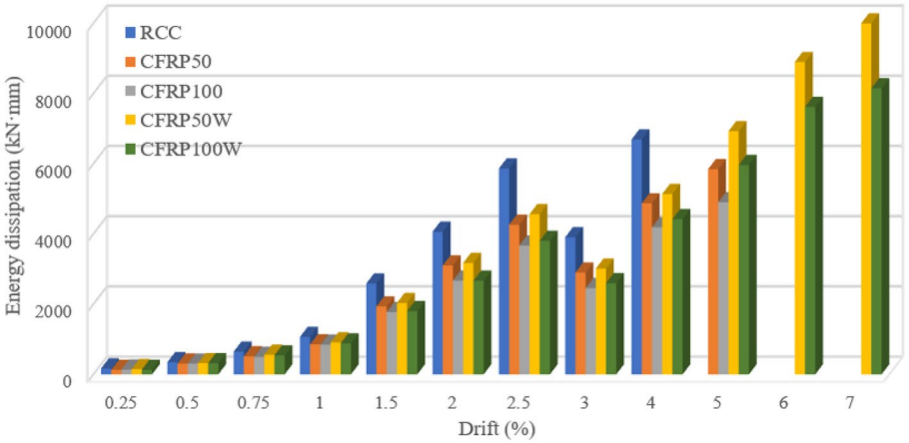

Fig. 15 The calculations of energy dissipation in different interstory drift

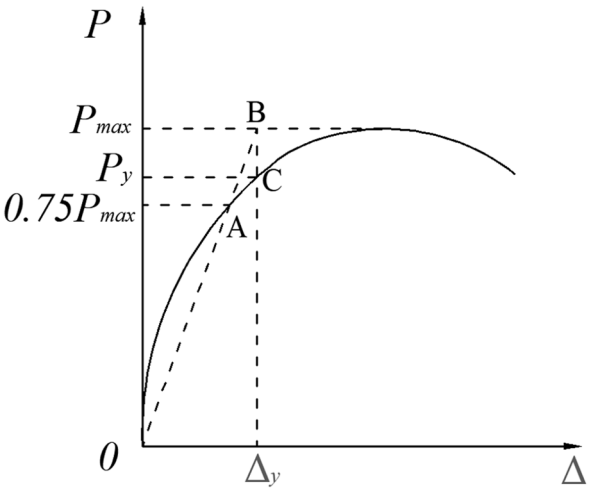

Fig. 16 Yield displacement calculation method

the specimens without CFRP sheets and the increment was related to interstory drift. The increment was about 5.5% when the interstory drift was 4% and was about 20% when the interstory drift was 5%. Comparing with the cumulative energy dissipation of specimen, the cumulative energy dissipation of CFRP100 specimen approximately descended 11.3%.

CFRP50W and CFRP100W showed excellent energy dissipation capacity: the cumulative energy dissipations were 88.9% and 85.8% higher than CFRP50 and CFRP100 specimens, 91.3% and 64.8% higher than RCC specimen, respectively. The result showed that CFRP sheets reinforcement could dramatically increase the energy dissipation capacities of specimens, remedy the imperfection of low energy dissipation in CFRP bars reinforced columns and improve the seismic performances of specimens.

3.8 The Ductility

The ductility coefficient can be calculated by the ratio of the ultimate displacement to the yield displacement. The yield displacement can be determined using the method proposed by Park [46].

The load of point A in the skeleton curve was 75% of the peak load. Connected point A and point 0 as an extension line and intersect the horizontal line of the peak load to obtain point B. The vertical line from point B intersected the skeleton curve to obtain point C. The load and displacement corresponding to point C were the yield load and yield displacement. The calculation method was shown in Fig. 16 and the calculation results were shown in Table 8.

Table 8 The calculation results of yield displacement and ductility

Specimens	RCC	CFRP50	CFRP100	CFRP50W	CFRP100W
Yield load (kN)	66.1	72.6	90.9	85.5	110.4
Ultimate displacement (mm)	52.8	66.0	66.0	92.4	92.4
Yield displacement (mm)	8.9	14.6	26.2	25.2	44.4
Ductility	5.9	4.5	2.5	3.7	2.1

It can be seen from Table 8, the ductility of CFRP50 specimen and CFRP100 specimen respectively decreased by 23.7% and 57.6% compared with RCC specimen, and the ductility of CFRP50W specimen and CFRP100W specimen further decreased 17.8% and 16% compared with specimens without CFRP sheets. Then the specimen reinforced by steel bars had the best ductility. The CFRP bars with the linear mechanical characteristics decreased the ductility of the other 4 specimens even the CFRP sheets increased the ultimate displacements.

4 Conclusions

In this paper, five circular columns reinforced with CFRP bars and CFRP sheets had been tested under the low-cyclic reversed load to discuss the effect of CFRP bars and CFRP sheets on the self-centering performance of the columns. The seismic performances of concrete circular columns were researched by analyzing the hysteresis curves, stiffness degradation, residual deformation, etc. The main conclusions were as follows:

1) CFRP bars can effectively improve the carrying capacity of the concrete circular columns. CFRP bars and CFRP sheets can increase the carrying capacities and the deformation capacities of specimens. The ultimate carrying loading and interstory drift of CFRP100W specimen are 21.5% and 40% higher than that of CFRP100 specimen, respectively.

2) Concrete circular columns reinforced with CFRP bars and CFEP sheets have the excellent self-centering capacity, residual deformation recovery rates of CFRP50W and CFPR100W are up to 56.8% and 78.5% which are significantly higher than 31.8% of RCC specimen.

3) CFRP bars have a certain improvement of stiffness degradation of concrete circular columns under large interstory drift: the residual stiffness of CFRP100 specimen is 47.9% higher than that of RCC specimen. At the same time, the residual stiffness of specimens which strengthening partially with CFRP sheets increase about 48% than specimens without CFRP sheets.

4) The energy dissipation capacities of the specimens are limited by the CFRP bars due to the linear elastic behaviors. However, CFRP sheets can remedy the imperfection of low energy dissipation caused by CFRP bars. The cumulative energy dissipation of CFRP50W and CFRP100W specimens are 91.3% and 64.8% higher than RCC specimen, respectively.

5) The ductility of CFRP100 specimen is 57.6% lower than that of RCC specimen. The CFRP reinforced specimens have less ductility even the CFRP bars and CFRP sheets increased the ultimate displacements.

Limitations of the experiment are worthy of further research. For example, the seismic performance test of specimens under a high axial compression ratio was not researched.

Acknowledgments Experimental work described in this paper was financially supported by the National Natural Science Foundation of China (Grant No. 12002317), the National Key R&D Program of China (2016YFE0125600), Program for Innovative Research Team of Education Ministry of China (IRT_16R67), Thousand Talents Plan in Henan Province (ZYQR201912029), and Key Science and Technology Program of Henan Province (212102310003).

Author Contributions Conceptualization: Jun Zhao, Xiaohui Ruan, Xinglong Gong; Methodology: Jun Zhao, Wenbo Ren, Chenzhe Si; Formal analysis and investigation: Wenbo Ren, Xiaohui Ruan, Chenzhe Si; Writing - original draft preparation: Jun Zhao, Wenbo Ren, Xiaohui Ruan; Writing - review and editing: Jun Zhao, Xiaohui Ruan; Funding acquisition:Jun Zhao, Xiaohui Ruan; Supervision: Jun Zhao, Xiaohui Ruan.

Data Availability The datasets generated during and analyzed during the current study are available from the corresponding author on reasonable request.

References

1. Liossatou, E., Fardis, M.N.: Residual displacements of RC structures as SDOF systems. Earthq. Eng. Struct. D. **44**, 713–734 (2015). https://doi.org/10.1002/eqe.2483
2. Report of the seventh joint planning meeting of NEES/E-defense collaborative research on earthquake engineering. PEER 2010/109. Berkeley. University of California. Berkeley. (2010)
3. McCormick, J., Aburano, H., Ikenaga, M.: Permissible residual deformation levels for building structures considering both safety and human elements. Proceedings of the 14th world conference on earthquake engineering. Beijing, China. 12-17 Oct (2008)
4. Astanehasl, A., Shen, J. H.: Rocking behavior and retrofit of tall bridge piers. Structural engineering in natural hazards mitigation. ASCE. (1993)
5. Wada, A., Qu, Z., Ito, H.: Seismic Retrofit Using Rocking Walls and Steel Dampers. ATC & SEI 2009 Conference on Improving the Seismic Performance of Existing Buildings and Other Structures. San Francisco, California. USA. (2009). https://doi.org/10.1061/41084(364)92
6. Stevenson, M., Korolyk, M.: Post-Tensioned Concrete Walls and Frames for Seismic-Resistance-A case study of the David Brower Center. SEAOC 2008 Convention Proceedings. (2008). https://doi.org/10.13140/2.1.2211.1686
7. Priestley, M. J. N., MacRae, G. A.: Seismic tests of precast beam-to-column joint subassemblages with unbonded tendons. Pci. Journal. **41**(1), 64-81 (1996). https://doi.org/10.15554/pcij.01011996.64.81
8. Ricles, J. M., Sause, R., Peng, S. W.: Experimental evaluation of earthquake resistant post-tensioned steel connections. J. Struct. Eng. **128**, 850-859 (2002). https://doi.org/10.1061/(ASCE)0733-9445(2002)128:7(850)
9. Kurama, Y., Sause, R., Pessiki, S.: Lateral load behavior and seismic design of unbonded post-tensioned precast concrete walls. ACI. Struct. J. **96**(4), 622-633 (1999). https://doi.org/10.14359/700
10. Kurama,Y. C.: Seismic design of unbonded posttensioned precast concrete walls with supplemental viscous damping. ACI. Struct. J. **97**(4), 648-658 (2000). https://doi.org/10.14359/7431
11. Sun, Y., Funato, Y.: Earthquake-resisting properties and evaluation of high-performance concrete columns with low residual deformation. Proceedings of 2015 World Conference on Control, Electronics and Electrical Engineering (WCEE 2015). Lisbon, Portugal. (2012)
12. Gu, A.Q., Zhou, Y., Xiao, Y.: Experimental study and parameter analysis on the seismic performance of self-centering hybrid reinforced concrete shear walls. Soil. Dyn. Earthq. Eng. **116**, 409–420 (2019). https://doi.org/10.1016/j.soildyn.2018.10.003
13. Cheng, C.T.: Shaking table tests of a self-centering designed bridge substructure. Eng. Struct. **30**, 3426–3433 (2008). https://doi.org/10.1016/j.engstruct.2008.05.017
14. Kalliontzis, D., Schultz, A.E.: Characterizing the In-Plane Rocking Response of Masonry Walls with Unbonded Posttensioning. J. Struct. Eng. **143**, 1–16 (2017). https://doi.org/10.1061/(ASCE)ST.1943-541X.0001838
15. Lee, W.K., Billington, S.L.: Performance-based earthquake engineering assessment of a self-centering, post-tensioned concrete bridge system. Earthq. Eng. Struct. Dyn. **40**, 887–902 (2010). https://doi.org/10.1002/eqe.1065
16. Darain, K.H., Mahfuz, U.D.: Strengthening of RC Beams Using Externally Bonded Reinforcement Combined with Near-Surface Mounted Technique. Polymers. **8**(7), 261 (2016). https://doi.org/10.3390/polym8070261
17. Bischof, P., Suter, R., Chatzi, E.: On the Use of CFRP Sheets for the Seismic Retrofitting of Masonry Walls and the Influence of Mechanical Anchorage. Polymers. **6**(7), 1972–1998 (2014). https://doi.org/10.3390/polym6071972
18. Demir, C., Kucukkapili, A., Doyrangol, D.: The Effects of Loading Rate and Duration on the Axial Behavior of Low-Strength and Medium-Strength Noncircular Concrete Members Confined by Fiber-Reinforced Polymer Sheets. Polymers. **6**(6), 1685–1704 (2014). https://doi.org/10.3390/polym6061685
19. Minkwan, J., Hongseob, O., Jongsung, S.: Indirect fatigue evaluation of CFRP-reinforced bridge deck slabs under variable amplitude cyclic loading. Ksce. J. Civ. Eng. **21**(5), 1783–1792 (2017). https://doi.org/10.1007/s12205-016-1494-1
20. Suriyati, R., Djauhari, Z.: Seismic performance of building reinforced with CFRP bars. Matec. Web. Con. **276**, (2019). https://doi.org/10.1051/matecconf/201927601021

21. Elrefai, A., West, J., Soudki, K.: Fatigue of reinforced concrete beams strengthened with externally post-tensioned CFRP tendons. Con. Build. Mate. **29**, 246–256 (2012). https://doi.org/10.1016/j.conbuildmat.2011.10.014
22. Ammar, F., Latief, A., Yasir, A.: Structural Behavior of Hybrid Reinforce Concrete Columns. J. Eng. Appl. Sci. **13**(23), 9813–9824 (2018). https://doi.org/10.3923/jeasci.2018.9813.9824
23. Zhang, L., Chen, J., Jiang, S.Y.: Performance of a transfer beam with hybrid reinforcement of CFRP bars and steel bars under reversed cyclic loading. Sci. Eng. Compos. Mater. **24**(4), 621–630 (2017). https://doi.org/10.1515/secm-2015-0035
24. Sharbatdar, M. K.: Concrete columns and beams reinforced with FRP bars and grids under monotonic and reversed cyclic loading. Ottawa, Canada: Ottawa Carleton Institute for Civil Engineer, **65**(3), 1452 (2003). https://doi.org/10.20381/ruor-19576
25. Zhong, K., Cai, D. Y., Wang, Z., Wang, T.: Full-scale seismic testing of concrete building columns reinforced with both steel and CFRP bars. Compo. Struct. **178**(Oct), 195-209 (2017). https://doi.org/10.1016/j.compstruct.2017.06.020
26. Zhao, J., Shen, F., Si, C.: Experimental Investigation on Seismic Resistance of RC Shear Walls with CFRP Bars in Boundary Elements. Int. J. Con. Struct. Mater. (2020). https://doi.org/10.1186/s40069-019-0377-5
27. Sokkary, H.E., Galal, K.: Seismic Behavior of RC Shear Walls Strengthened with Fiber-Reinforced Polymer. J. Compos. Constr. **17**(5), 603–613 (2013). https://doi.org/10.1061/(ASCE)CC.1943-5614.0000364
28. Salleh, N., Mohd, Sam. A. R., Mohd, Yatim. J.: Flexural Behavior of GFRP RC Beam Strengthened with Carbon Fiber Reinforced Polymer (CFRP) Plate: Cracking Behavior. App. Mech. Mater. **752-753**, 610-616 (2015). https://doi.org/10.4028/www.scientific.net/AMM.752-753.610
29. Saljoughian, A., Mostofinejad, D., Hosseini, S.: M: CFRP confinement in retrofitted RC columns via CSB technique under reversed lateral cyclic loading. Mater. Struct. **52**(4), 1–14 (2019). https://doi.org/10.1617/s11527-019-1373-6
30. Hamid, S.: Extending service life of concrete and masonry structures with fiber composites. Constr. Build. Mater. **11**(5/6), 327–335 (1997). https://doi.org/10.1016/S0950-0618(97)00054-8
31. Saqan, E. I., Rasheed, H. A., Alkhrdaji, T.: Evaluation of the seismic performance of reinforced concrete frames strengthened with CFRP fabric and NSM bars. Compos. Struct. **184**(JAN), 839-847 (2017). https://doi.org/10.1016/j.compstruct.2017.10.069
32. Wang, J. Z., Yang, J. L., Cheng, L.: Experimental Study on the Seismic Behavior of High-strength Reinforced Concrete Columns Strengthened with CFRP under Cyclic Loading. J. Struct. Eng. **145**, (2019). https://doi.org/10.1061/(ASCE)ST.1943-541X.0002251
33. Yang, J. L., Wang, J. Z.: Seismic Performance of Shear-Controlled CFRP-Strengthened High-Strength Concrete Square Columns under Simulated Seismic Load. J. Compos. Constr. **22**, (2018). https://doi.org/10.1061/(ASCE)CC.1943-5614.0000901
34. Wang, D., Huang, L., Yu, T.: Seismic Performance of CFRP-Retrofitted Large-Scale Square RC Columns with High Axial Compression Ratios. J. Compos. Constr. **21**, (2017). https://doi.org/10.1061/(ASCE)CC.1943-5614.0000813
35. Ye, L. P., Zhang, K., Zhao, S. H.: Experimental study on seismic strengthening of RC columns with wrapped CFRP sheets. Constr. Build. Mater. **17**(6), 499–506 (2001). https://doi.org/10.1016/S0950-0618(03)00047-3
36. Saljoughian. A., Mostofinejad. D: Using grooving and corner strip-batten techniques for seismic strengthening of square reinforced concrete columns with fiber-reinforced polymer composites. Struct. Concr. **21**(5), (2020). https://doi.org/10.1002/suco.201900459
37. Saljoughian. A., Mostofinejad. D: Grooving methods in square RC columns strengthened with longitudinal CFRP under cyclic axial compression. Eng. Struct. **174**, 724–735, (2018). https://doi.org/10.1016/j.engstruct.2018.08.007
38. Zhang, Y. Y., Ma, Y., Paolo, G.: Seismic performance of precast segmental bridge columns repaired with CFRP wraps. Compos. Struct. **243**, (2020). https://doi.org/10.1016/j.compstruct.2020.112218
39. GB50107-2010: Standard for evaluation of concrete compressive strength. Beijing, China. (2010) (in Chinese)
40. GB50010-2010: Code for design of concrete structures. Beijing, China. (2010) (in Chinese)
41. GB50550-2010: Code for acceptance of constructional quality of strengthening building structures. Beijing, China. (2010) (in Chinese)
42. JGJ/T101-2015: Specification for seismic test of buildings. Beijing, China. (2015) (in Chinese)
43. JGJ3-2010: Technical specification for concrete structure of tall building. Beijing, China. (2011) (in Chinese)

44. Song, M. R., Liu, B. K., Huang, S. J: Experimental Study of Seismic Performance on Three-Story Prestressed Fabricated Concrete Frame. Adv. Mater. Res. 250-253, (2011). https://doi.org/10.4028/www.scientific.net/AMR.250-253.1287
45. Lei, Z., Qu, J. T., Su, Y., Liu, Y.: Mechanical behaviour of masonry walls strengthened by BFRP composites. Mater. Res. Innovations. **19**(suppl.5), (2015). S5-1077-S5-1082. https://doi.org/10.1179/1432891714Z.0000000001252
46. Park, R.: Evaluation of ductility of structures and structural assemblages from laboratory testing. Bulletin of the New Zealand Society for Earthquake Engineering **22**(3), 155–166 (1989). https://doi.org/10.5459/bnzsee.22.3.155-166
47. Mostofinejad, D., Akhlaghi, A: Experimental investigation of the efficacy of EBROG method in seismic rehabilitation of deficient reinforced concrete beam–column joints using CFRP sheets. J. Compos. Constr. **21**(4), (2017). https://doi.org/10.1061/(ASCE)CC.1943-5614.0000781